Computational microscopy with the PERCIVAL detector system at TwinMic beamline

Published by IOP Publishing for Sissa Medialab

Received: *September 29, 2024*
Accepted: *December 21, 2024*
Published: *January 24, 2025*

25th International Workshop on Radiation Imaging Detectors
Lisbon, Portugal
30 June – 4 July 2024

Computational microscopy with the PERCIVAL detector system at TwinMic beamline

Francesco Guzzi[a,*] **Alessandra Gianoncelli**[a] **Luigi Stebel**[a] **Dario Giuressi**[a] **Giuseppe Cautero**[a] **Roberto Borghes**[a] **Iztok Gregori**[a] **Fulvio Billè**[a] **Martin Scarcia**[a] **Valentina Bonanni**[a] **Milan Žižić**[a] **HyoJung Hyun**[b] **William Nichols**[c] **Jonathan Correa**[d,e] **Alessandro Marras**[d,e] **Cornelia B. Wunderer**[d,e] **Heinz Graafsma**[d,e,f] **Ralf Hendrik Menk**[a] **and George Kourousias**[a]

[a] *Elettra Sincrotrone Trieste S.C.p.A, Strada Statale 14, Basovizza (Trieste), Italy*
[b] *Pohang Accelerator Laboratory (PAL), 80 Jigokro-127-beongil, Pohang, Republic of Korea*
[c] *Diamond Light Source, Harwell Science and Innovation Campus, Didcot, U.K.*
[d] *Deutsches Elektronen-Synchrotron DESY, Notkestraße 85, Hamburg, Germany*
[e] *Center for Free-Electron Laser Science CFEL, Luruper Ch 149, Hamburg, Germany*
[f] *Mid-Sweden University, 852 30 Sundsvall, Holmgatan, Sweden*

E-mail: francesco.guzzi@elettra.eu

Abstract: PERCIVAL is a novel soft X-ray detection system designed for the needs of modern microscopy. By integrating it into the TwinMic end-station at Elettra Sincrotrone Trieste, we conducted an exploratory computational microscopy experiment on biological samples, aiming at evaluating the entire system in a real use-case scenario. We present the methodology to convert the RAW data and our high-resolution image reconstructions.

Keywords: Data processing methods; Image reconstruction in medical imaging; X-ray detectors

*Corresponding author.

https://doi.org/10.1088/1748-0221/20/01/C01032

2025 JINST 20 C01032

Contents

2025 JINST 20 C01032

1 Introduction

Soft X-ray microscopy [1] offers nanoscale imaging with exceptional contrast, enabling in situ and in operando studies of biological and materials science samples [1]. Advances in computational approaches such as Coherent Diffraction Imaging (CDI) [2–4] enabled high-resolution and quantitative phase microscopy, while also simplifying the experimental setup, which is often defined lensless [5]. However, the shift toward computational methods emphasizes the importance of a reliable data acquisition, as the processing pipeline is tailored on specific properties of the sensing mechanisms (computational imaging).

PERCIVAL (Pixelated Energy Resolved CMOS Imager, Versatile And Large) [6–10] is a new soft-X-ray detector system designed for the needs of modern soft-X-ray microscopy experiments [7] performed at synchrotron facilities [9]. Developed collaboratively by six research institutes (DESY, RAL/STFC, Elettra, DLS, PAL and SOLEIL [7], this detector is now at an advanced stage, featuring a Back-Side-Illuminated (BSI) sensor [7, 9], fast acquisition/conversion electronics, and specialised control software. It represents a novel and advanced detection system that should improve existing computational microscopy techniques and potentially inspire new ones.

In this paper, we report on an exploratory soft-X-ray imaging experiment at the TwinMic synchrotron radiation beamline [11, 12] in Elettra Sincrotrone Trieste (Trieste, Italy), exploiting the latest version of the PERCIVAL detector system [9]; we evaluated its performances, in a real use-case scenario, where the detector is employed to reconstruct at *real-time* both transmission and phase images, encompassing biological and test-pattern samples. By leveraging on the collaboration and the experience gained during previous experiments with PERCIVAL reported in [7, 9] and the flexibility of the TwinMic end-station [11], we were able to fully exploit the system's high speed, the high-dynamic-range of the sensor and its large area.

2 Background

The TwinMic end-station operates in the 400–2200 eV energy range [11, 12], supporting both X-ray fluorescence spectromicroscopy and Scanning Transmission X-ray Microscopy (STXM); a single Fresnel Zone Plate (FZP) creates a nanoprobe and the sample is raster-scanned (in $\hat{x}$ and $\hat{y}$) across it (see figure 1). By measuring the transmitted light intensity at each position, an absorption map can be generated [13]. Utilisation of a 2D detector enables the computation of spatial moments [14], which add different qualitative phase-contrast modalities [1]. For this setup, detector speed is crucial [11], as

each frame corresponds to one pixel in the resulting absorption or Differential Phase Contrast (DPC) map. The real-time nature of both, acquisition and processing of such maps, is essential to efficiently navigate on the sample areas of interest and to drive further coherent-diffraction centric experiments.

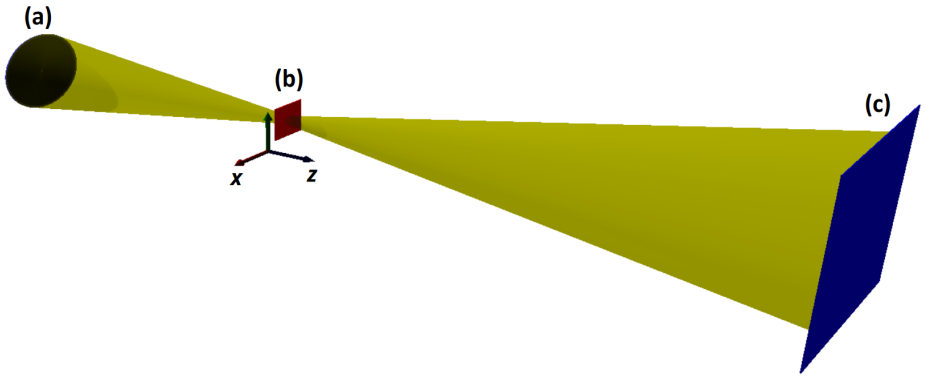

Figure 1. Schematization of the direct X-ray detection TwinMic setup with the Fresnel Zone Plate (a) producing a nanoprobe on the sample plane (b). The inline hologram and the diffraction pattern are acquired on the detector plane (c), positioned along the optical axis $\hat{z}$.

PERCIVAL is a modern detector system designed to satisfy a large number of CDI methods requirements. It has been described in detail [6, 7] and evaluated at different development stages [6–8, 10] in different works. Unlike previous experiments performed at Elettra [8], a descrambling board is inserted in the acquisition chain between the mezzanine card [6] and the Linux workstation, allowing the reordering of data via fast hardware-based algorithms. Specific network workarounds have been implemented at software level, such that raw image data are acquired via two 10 Gb/s optical connections, directly and without the need of an expensive hardware deep buffer switch. The Linux camera server [10] is used to coordinate the acquisition and data collection processes: it consists of several modules, with the primary components being the camera controller (receiving commands from the beamline TANGO control system), two frame receivers (one for each connection) and two file writers, which work in tandem to efficiently acquire and store the data at high-speed [10].

3 Methods

In order to obtain conventional images, each stack of frames — consisting of RAW 16-bit codewords — requires further levels of processing before data can be correctly interpreted. The sensor can be operated both in single or adaptive gain mode, eventually expanding the overall dynamic range at the cost of increased complexity in processing. The use of multiple gains requires that a specific set of calibration data for each individual gain must be used. On-chip Analog-to-Digital Converters (ADC), based on a Two-Step Single Slope (TS-SS) architecture [6], use two different current ramps (fast and slow) and a threshold logic to provide corresponding Coarse C and Fine F values for each pixel. The final 16-bit codewords combine these information representing for each pixel the selected value of gain (G, 2 bits), the ADC coarse counter (C, 5 bits), and the ADC fine counter (F, 8 bits). A very rough and preliminary intensity image can be obtained by simply multiplying the gain value by the coarse counts, thus totally discarding the F information and in most cases having a constant value for G (fixed gain mode or limited dynamic range). On the other hand, to fully exploit the detector capabilities, proper ADC calibration

2025 JINST 20 C01032

weights should be applied [7–9]. The sensor features 7 independent ADCs for each of the 1440 columns of the sensor. The procedure to obtain the ADC calibration parameters requires collecting a special set of dark scan images and estimating linear fits (slope S and offset O) for all of the fast (coarse — subscript c) and slow (fine — subscript f) voltage-to-ADU ramps. The four calibration values (S_c, S_f, O_c, O_f) are then used in eq. (3.1) [7, 9] for the actual conversion to ADU values denoted by V:

$$V = O + S_c \times (C + 1 - O_c) - S_f \times (F - O_f) \tag{3.1}$$

where O is a global voltage offset. Operating in this way it is possible to account for pixel-to-pixel variations and obtain "conventional" frames, including dark measurements used for the pedestal subtraction.

By applying eq. (3.1) on the RAW measurements, the frames become ready to be used in a conventional way; the same step is used for any type of frame acquired by the camera system, including dark measurements used for the pedestal subtraction. For a STXM dataset, the inline hologram feature ("donut") [11] is cropped and is used to compute the spatial zeroth (absorption), first (DPC) and second (dark contrast) central moment for each acquired image [1, 14]. The outcome of these calculations (performed for each frame) is then mapped to a corresponding point in a 2D space, reflecting the sample stage movements. The horizontal and vertical DPC map can subsequently be processed through a Fourier derivative method to produce an approximate integral phase contrast image [15], following eq. (3.2)

$$\hat{\Phi} = Re\left\{ j \cdot \mathbf{F}^{-1}\left\{ \frac{q_x \mathbf{F}\{\Phi_x\} + q_y \mathbf{F}\{\Phi_y\}}{q_x^2 + q_y^2} \right\} \right\} \tag{3.2}$$

where j is the imaginary unit, q_x and q_y are the coordinates in the Fourier space, Φ_x and Φ_y are respectively the horizontal and vertical DPC maps and $\mathbf{F}$ and $\mathbf{F}^{-1}$ are the forward and inverse Fourier Transform. The output $\hat{\Phi}$ is a real-valued map representing the phase of the complex-valued 2D sample transmission function.

4 Results

For the reported experiment, the camera was positioned approximately at 30 cm from the rear of the TwinMic end-station (90 cm from the sample) and connected to the microscope port via a flexible pipe. The sensor was cooled down to −20 °C once the pressure at the camera port was stabilised to 10^{-5} mbar. Although the cooling system could achieve lower temperatures, the sensor's performance specifications at this temperature seemed to be reliable. The sample and optics chamber of the microscope were maintained at a steady pressure of 10^{-6} mbar. Once the temperature stabilized, several datasets were acquired at an energy of 1515 eV.

Figure 2 presents a comparison between images obtained using the standard DV860 ANDOR technology camera of TwinMic beamline [11]) and those computed from PERCIVAL data, as it was possible to switch from one camera to the other one by moving some optical element without breaking the vacuum. The sample depicted in figure 2 was a 10 µm thick slice of bread [17] imaged in an area of 80 × 80 µm with a step size of 1 µm and a dwell time of 12 ms for PERCIVAL and 20 ms the Andor CCD respectively. The light gray rectangular area, denoting lower absorption than the surrounding area (panel a and d) is the result of radiation damage caused during a previous experiment [17]. As expected, there is no significant improvement in the resolution of these maps, given the nature of the STXM data acquisition process. However, when comparing DPC images (panel b-e and c-f), the ones

2025 JINST 20 C01032

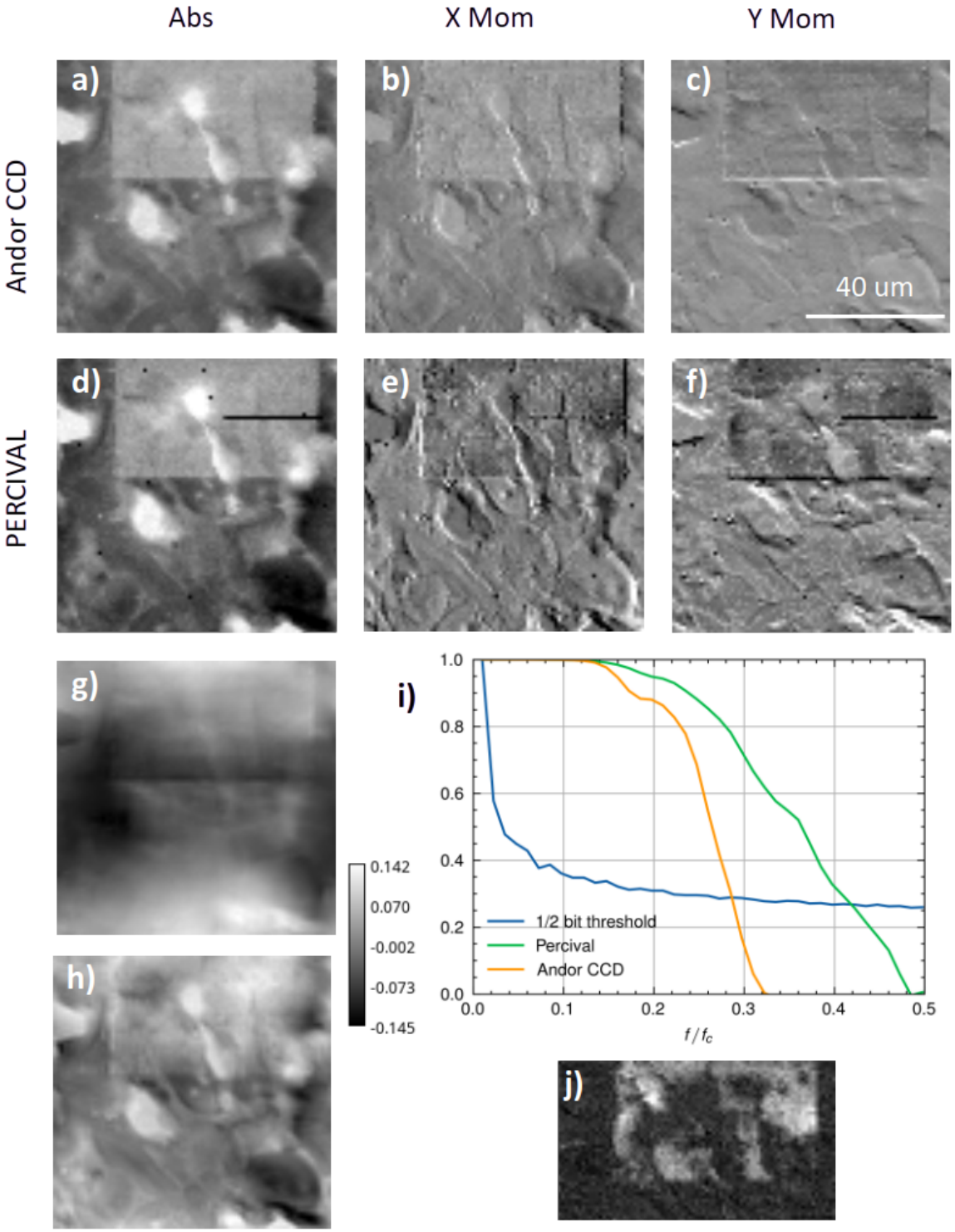

Figure 2. Comparison of STXM images, absorption (a,d), differential phase contrast in $\hat{x}$ (b,e) and in $\hat{y}$ (c,f) and phase reconstruction (g,h) obtained with the ANDOR CCD camera (used in the typical Twinmic experiments [11]) and the ones computed from PERCIVAL data respectively. Panel (i) shows the single-image Fourier Ring Correlation (FRC) curves [16] computed for panel (g,h), demonstrating a clear increase in image resolution (intercept with the half-bit curve). Panel (j) shows the dark-contrast image, computed by analyzing the central moment of order 2 on the diffraction patterns.

2025 JINST 20 C01032

computed from PERCIVAL data demonstrate higher contrast (panel c and f). This improvement is attributed to the detector's larger area, higher pixel count, and direct X-ray detection, which allowed for a more accurate estimation of the distribution centroid. In contrast, the absorption images show no noticeable enhancement (panel a and d), as the experimental conditions were already optimized to provide a high signal-to-noise ratio in both cases for the zeroth moment. The high-SNR DPC data obtained from PERCIVAL, allowed us to compute the integral phase with the Fourier-based filtering method in [15], producing a convincing phase image (panel h) which is definitely more informative then the one obtained by processing the Andor data (panel g). The resolution of panel g and h can be estimated with the single-image Fourier Ring Correlation (FRC) method [16] (figure 2 panel i) which denotes a well-defined increase in the amount of information which can be extracted from the image (intercept with the half-bit curve). In order to obtain meaningful results, it was essential to inpaint [18] the defective areas in each of the DPC maps. Finally, the dark field image computed from the second order statistics on the frames suggest higher scattering in the area of the radiation damage (panel j).

Figure 3 shows the same methodology applied on a different sample — a nickel siemens star — scanned with a probe size of 500 nm. The entire area of 20×20 µm pixels covering one quarter of the test pattern is represented by 1600 pixels. Panel (a), (b) and (c) represent respectively the absorption and DPC images computed on the Andor frames, while panels d-f displays the results obtained with the PERCIVAL camera system. Similarly to the previous case, panel g shows the phase map obtained with the PERCIVAL data, where alterations in the regularity of the silicon nitride substrate are made

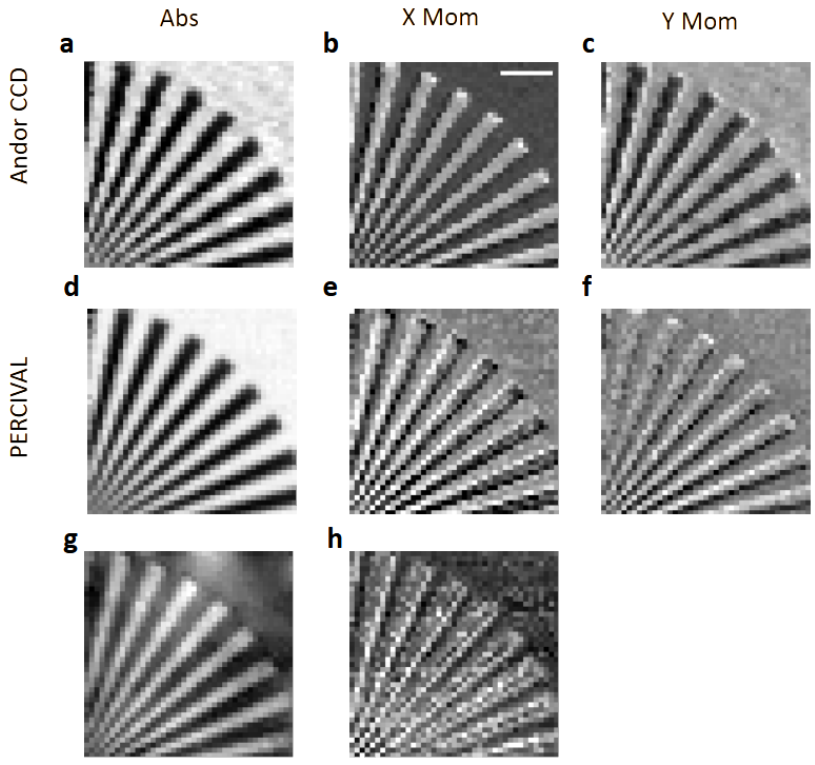

Figure 3. STXM images of a siemens star test-sample (area of 20×20 µm scanned with a probe size of 500 nm); panels (a,d) represent the absorption images while (b,e) and (c,f) the differential phase contrast images in X and Y respectively, acquired with the Andor (a to c) and PERCIVAL (d to f) cameras; panels (g) and (h) show the Fourier-filtered integral phase and the dark-field contrast images respectively. The white bar in panel (b) is 5 µm long.

2025 JINST 20 C01032

evident by the phase part of the sample transmission function. Edge sensitivity is instead expected in panel h, depicting the dark-contrast, computed on the PERCIVAL frames.

From the usability point of view, PERCIVAL is clearly not designed and not optimised for STXM-like measurements, as a large area of the frame is wasted, not being used in the computation. Moreover, even the transfer of just two (reset and sample) full (1484×1440 pixels) image frames for each point of a typical STXM map (100×100 points) results in a total of about 85 GB of RAW data that need to be streamed out efficiently and reliably, before undergoing any pre-processing. The use of PERCIVAL also for STXM-like measurements is hovewer desirable and would strongly benefit from some foreseen hardware improvements, such as Region Of Interest and binning capabilities. This may speed up the measurement and ease the data handling for image reconstruction.

5 Conclusions and outlook

In this paper, we presented the results from the first user beamtime utilising the PERCIVAL detector system at TwinMic (Elettra Sincrotrone Trieste) following significant updates to the sensor, the electronics, and the control software. We successfully acquired and reconstructed both transmission and phase images from biological and test-pattern specimens, demonstrating the detector's potential for these applications, particularly for CDI and ptychography. However, we identified areas for improvement, including the absence of ROI/binning capabilities, noticeable spatial noise, and the need for a cumbersome manual calibration of acquired data. Future work will focus on addressing these issues to enhance the system's performance.

References

[1] B. Kaulich, P. Thibault, A. Gianoncelli and M. Kiskinova, *Transmission and emission x-ray microscopy: operation modes, contrast mechanisms and applications*, *J. Phys. Condens. Matter* **23** (2011) 083002.

[2] D. Shapiro et al., *Biological imaging by soft x-ray diffraction microscopy*, *Proc. Nat. Acad. Sci.* **102** (2005) 15343.

[3] H.N. Chapman and K.A. Nugent, *Coherent lensless X-ray imaging*, *Nature Photon.* **4** (2010) 833.

[4] D.J. Vine et al., *Ptychographic Fresnel coherent diffractive imaging*, *Phys. Rev. A* **80** (2009) 063823.

[5] F. Pfeiffer, *X-ray ptychography*, *Nature Photon.* **12** (2017) 9.

[6] C.B. Wunderer et al., *The PERCIVAL soft X-ray imager*, 2015 *JINST* **10** C02008.

[7] A. Marras et al., *Characterization of the Percival detector with soft X-rays*, *J. Synchrotron Radiat.* **28** (2021) 131.

[8] G. Pinaroli et al., *PERCIVAL: possible applications in X-ray micro-tomography*, 2020 *JINST* **15** C02007.

[9] J. Correa et al., *The PERCIVAL detector: first user experiments*, *J. Synchrotron Radiat.* **30** (2023) 242.

[10] A. Palaha et al., *Report on Control/DAQ Software Design and Current State of Implementation for the Percival Detector*, in the proceedings of the *15th International Conference on Accelerator and Large Experimental Physics Control Systems*, Melbourne, Australia, 17–23 October 2015 [DOI:10.18429/JACoW-ICALEPCS2015-MOPGF070].

[11] A. Gianoncelli et al., *Current status of the TwinMic beamline at Elettra: a soft X-ray transmission and emission microscopy station*, *J. Synchrotron Radiat.* **23** (2016) 1526.

2025 JINST 20 C01032

[12] A. Gianoncelli et al., *Soft X-ray Microscopy Techniques for Medical and Biological Imaging at TwinMic-Elettra*, *Appl. Sci.* **11** (2021) 7216.

[13] A. Gianoncelli et al., *Scanning transmission x-ray microscopy with a configurable detector*, *Appl. Phys. Lett.* **89** (2006) 251117.

[14] G. Morrison, W.J. Eaton, R. Barrett and P. Charalambous, *STXM imaging with a configured detector*, *J. Phys. (France) IV* **104** (2003) 547.

[15] M.D. de Jonge et al., *Quantitative Phase Imaging with a Scanning Transmission X-Ray Microscope*, *Phys. Rev. Lett.* **100** (2008) 163902.

[16] B. Rieger et al., *Single image Fourier ring correlation*, *Opt. Express* **32** (2024) 21767.

[17] S. Sala et al., *Investigation of the spatial distribution of sodium in bread microstructure using X-ray, light and electron microscopy*, *LWT* **209** (2024) 116787.

[18] F. Guzzi et al., *Automatic Differentiation for Inverse Problems in X-ray Imaging and Microscopy*, *Life* **13** (2023) 629.

2025 JINST 20 C01032